Characterizing the Tropospheric Ozone Response to Methane Emission Controls and the Benefits to Climate and Air Quality

Arlene M. Fiore[1], J. Jason West[234], Larry W. Horowitz[1], Vaishali Naik[3], M. Daniel Schwarzkopf[1]

[1]NOAA Geophysical Fluid Dynamics Laboratory, Princeton, NJ, USA

[2]Atmospheric and Oceanic Sciences Program, Princeton University, Princeton, NJ, USA.

[3]Woodrow Wilson School of Public and International Affairs, Princeton University, Princeton, NJ, USA.

[4]Now at University of North Carolina at Chapel Hill, Chapel Hill, NC, USA.

Submitted to J. Geophys. Res., July 12, 2007
Revised November 2, 2007

Short title: Ozone Response to Methane

Keywords: methane, ozone, air quality

Index Terms:
Primary 0365 Troposphere: Composition and Chemistry
1) 0368 Troposphere: Constituent Transport and Chemistry
2) 0478 Pollution, urban, regional, and global
3) 0325 Evolution of the atmosphere
4) 1610 Global change atmospheres

Abstract

Reducing methane (CH_4) emissions is an attractive option for jointly addressing climate and ozone (O_3) air quality goals. With multi-decadal full-chemistry transient simulations in the MOZART-2 tropospheric chemistry model, we show that tropospheric O_3 responds approximately linearly to changes in CH_4 emissions over a range of anthropogenic emissions from 0-430 Tg CH_4 yr^{-1} (0.11-0.16 Tg tropospheric O_3 or ~11-15 ppt global mean surface O_3 decrease per Tg yr^{-1} CH_4 reduced). We find that neither the air quality nor climate benefits depend strongly on the location of the CH_4 emission reductions, implying that the lowest cost emission controls can be targeted. With a series of future (2005-2030) transient simulations, we demonstrate that cost-effective CH_4 controls would offset the positive climate forcing from CH_4 and O_3 that would otherwise occur (from increases in NO_x and CH_4 emissions in the baseline scenario) and improve O_3 air quality. We estimate that anthropogenic CH_4 contributes 0.7 Wm^{-2} to climate forcing and ~4 ppb to surface O_3 in 2030 under the baseline scenario. Although the response of surface O_3 to CH_4 is relatively uniform spatially compared to that from other O_3 precursors, it is strongest in regions where surface air mixes frequently with the free troposphere and where the local O_3 formation regime is NO_x-saturated. In the model, CH_4 oxidation within the boundary layer (below ~2.5 km) contributes more to surface O_3 than CH_4 oxidation in the free troposphere. In NO_x-saturated regions, the surface O_3 sensitivity to CH_4 can be twice that of the global mean, with >70% of this sensitivity resulting from boundary layer oxidation of CH_4. Accurately representing the NO_x distribution is thus crucial for quantifying the O_3 sensitivity to CH_4.

1. Introduction

Methane (CH_4) emission controls are currently receiving attention as a viable low-cost strategy for abating surface ozone (O_3) pollution while simultaneously slowing greenhouse warming [*Hansen et al*., 2000; *Fiore et al*., 2002a; *Dentener et al*., 2005; *EMEP*, 2005; *West and Fiore*, 2005; *West et al*., 2006]. In the presence of nitrogen oxides (NO_x), tropospheric CH_4 oxidation leads to the formation of O_3 [*Crutzen,* 1973]. Over the last century, global background O_3 concentrations have risen by at least a factor of two, due mainly to increases in CH_4 and NO_x emissions [*e.g. Marenco et al*., 1994; *Wang and Jacob*, 1998]. Here, we characterize the response of tropospheric O_3 to controls on CH_4 emissions, analyze the dominant processes determining the distribution of this response, and quantify the resulting benefits to air quality and climate.

With a lifetime of approximately a decade, CH_4 is fairly well-mixed in the atmosphere. Sources of atmospheric CH_4 include wetlands, ruminants, energy, rice agriculture, landfills, wastewater, biomass burning, oceans, and termites. Anthropogenic emissions are estimated to contribute at least 60% to total CH_4 emissions, with individual studies reporting a range of 500 to 610 Tg yr^{-1} for total CH_4 emissions [*Denman et al*., 2007]. The dominant CH_4 sink is reaction with the hydroxyl radical (OH) in the troposphere. If sufficient quantities of NO_x are available, CH_4 oxidation produces O_3 via reactions of peroxy radicals with NO_x. In a low-NO_x environment, formation of methyl hydroperoxide (CH_3OOH) suppresses O_3 production and may provide a net O_3 sink. In an extremely low-NO_x environment, CH_4 oxidation may also decrease O_3 levels by HO_2 reacting preferentially with O_3 rather than with NO. Under present-day tropospheric conditions, however, *Spivakovsky et al*. [2000] show that HO_2+NO is more important than HO_2+O_3 globally as a source of OH (their Figure 10), implying that increases in CH_4 abundances should yield a net global increase in the tropospheric O_3 burden, as has been reported in prior modeling studies [*e.g. Prather et al*., 2001]. Previously, CH_4 and NO_x emission reductions have been shown to be the most effective means of lowering tropospheric O_3: reductions in anthropogenic NO_x emissions decrease surface O_3 in polluted source regions by up to four times more than equivalent percentage reductions in anthropogenic CH_4 emissions, while CH_4 reductions have a stronger impact on the

tropospheric O_3 burden, and a similar influence to NO_x on global average surface O_3 concentrations [*Fiore et al.*, 2002a; *West et al.*, 2007a].

To date, most chemical transport model (CTM) studies have applied a uniform CH_4 mixing ratio to avoid the computational expense of multi-decadal simulations required for CH_4 to reach a steady state [*e.g.*, *Prather et al.*, 2001; *Stevenson et al.*, 2006]. We have previously adopted this approach to evaluate the benefits to human health, agriculture, and commercial forests resulting from lower O_3 due to CH_4 emission reductions [*West and Fiore*, 2005; *West et al.*, 2006]. In such simulations, termed "steady-state" in our analysis below, the uniform CH_4 mixing ratio is adjusted to reflect a desired CH_4 emission change, accounting for the non-linear feedback of CH_4 on its own lifetime through OH [*Prather*, 1996; *Prather et al.*, 2001]. Since the relationship between CH_4 emissions and CH_4 concentrations is non-linear, it is important to assess the degree to which this non-linearity affects the accuracy of estimates obtained by scaling results (*e.g.*, changes in O_3 concentrations) from one CH_4 perturbation to another.

In Figure 1, we compile estimates of the response of tropospheric O_3 to changes in CH_4 emissions from several global CTMs in the literature, to investigate whether changes in O_3 scale linearly with changes in CH_4 emissions. We include results from transient, full-chemistry simulations [*Dentener et al.*, 2005], from "steady-state" simulations with a uniform, fixed CH_4 concentration [*Wang and Jacob*, 1998; *Prather et al.*, 2001; *Fiore et al.*, 2002a; *West et al.*, 2006, 2007a], and from a hybrid modeling approach [*Shindell et al.*, 2005]. Despite variations in the simulation type, the total CH_4 emissions, the anthropogenic fraction of CH_4 emissions, and the emissions of other species that affect OH, Figure 1 shows that the tropospheric O_3 burden responds roughly linearly to changes in anthropogenic CH_4 emissions across the models. Estimates from the individual studies range from 0.12-0.16 Tg tropospheric O_3 per Tg yr^{-1} change in CH_4 emissions. Although the feedback between CH_4 and OH will cause the CH_4 concentration to respond in a strongly non-linear manner for sufficiently large increases in CH_4 emissions, the relationship is approximately linear for the range of emission perturbations considered in Figure 1, corroborating earlier results derived from theory and applied in a one-box model [*Prather*, 1996]. We further estimate from the published studies in Figure 1 that anthropogenic CH_4 currently contributes ~50 Tg to the annual

mean tropospheric O_3 burden, and ~5 ppb to global mean surface O_3 (based on the subset of models reporting changes in surface O_3 [*Fiore et al*., 2002a; *Dentener et al*., 2005; *West et al*., 2006]).

Designing effective CH_4 controls to combat O_3 air pollution requires knowledge of the magnitude and spatial pattern of the surface O_3 response to changes in CH_4 emissions. The sensitivity of O_3 to changes in CH_4 should depend on the emission ratio of NO_x to non-methane volatile organic compounds (NMVOC) and carbon monoxide (CO), which affects the abundance of OH [*Wang and Jacob*, 1998; *West et al*., 2006]. Here, we apply the global MOZART-2 CTM to characterize the O_3 response to CH_4 emission changes both with and without changes in emissions of other species (NO_x, CO and NMVOC; Sections 3 and 4). We then examine the processes contributing to the regional pattern of the O_3 response to CH_4 (Section 5), and identify any dependence of this response on the geographical location of the CH_4 source (Section 6). Finally, we quantify the global and regional air quality (Section 7) and radiative forcing (Section 8) impacts that could be attained via CH_4 controls from 2005 to 2030.

2. Methane simulations

We apply the MOZART-2 global model of tropospheric chemistry [*Horowitz et al*., 2003] to assess the response of O_3 to changes in CH_4 emissions. Table 1 provides a summary of the twelve simulations used in our study, which are described in detail below. We first consider sustained CH_4 emission reductions in transient simulations in which other emissions are held fixed at present-day values (Section 2.1) in order to diagnose the CH_4-OH feedback factor in our model and to characterize the tropospheric O_3 response to CH_4 emission controls. We then apply CH_4 controls phased in between 2005 and 2030 along three different trajectories, relative to a baseline future emission scenario in which emissions of CH_4 and other O_3 precursors change (Section 2.2). These future scenarios in which CH_4 controls are implemented in a more plausible manner allow us both to quantify the climate and air quality benefits that could be attained via different policy options and to examine the extent to which these benefits can be scaled from one CH_4 control trajectory to another. Finally, we employ "steady-state" simulations (Section 2.3) to examine the relative impact of CH_4 oxidation in the free

troposphere versus in the boundary layer on surface O_3, and to quantify the total contribution of anthropogenic CH_4 to tropospheric O_3. All simulations are driven by meteorological fields from the NCEP reanalysis [*Kalnay et al*., 1996] at a horizontal resolution of 1.9° x 1.9° with 28 vertical levels. We update the isoprene nitrate chemistry, from the 8% yield [*Carter and Atkinson*, 1996] used by *Horowitz et al*. [2003] to 12% [*Sprengnether et al*., 2002], and treat isoprene nitrates as a NO_x sink [e.g., *Chen et al*., 1998]; this modification reduces the positive bias in the MOZART-2 surface O_3 simulation [*Murazaki and Hess*, 2006] as discussed further in Section 2.4. Our simulations focus exclusively on the role of changes in O_3 precursor emissions and do not include any impacts resulting from future changes in climate.

2.1 Transient Simulations of Sustained CH_4 Reductions

We conduct three full-chemistry transient simulations beginning in 1990, with emissions of all O_3 precursors, except for CH_4 (and the lightning NO_x source which is tied to the meteorology as in *Horowitz et al*. [2003]), held constant. In the first simulation (BASE), we maintain CH_4 emissions at 1990 levels. The BASE CH_4 emissions (Table 2) include 308 Tg yr^{-1} from anthropogenic sources [*Olivier et al*., 1996; 1999] and 25 Tg yr^{-1} from biomass burning [*Horowitz et al*., 2003]. We uniformly increase the global wetland emissions from *Horowitz et al*. [2003] by 40% to 204 Tg yr^{-1} on the basis of recent estimates [*Wang et al*., 2004]. The 1990-2004 winds are recycled to complete 30-year simulations.

Since we wish to investigate the sensitivity of O_3 to the geographical location of CH_4 emissions, we conduct two additional simulations, in both of which global anthropogenic CH_4 emissions are decreased by the same magnitude. In one simulation (RASIA), we set Asian (India, East Asia, and Southeast Asia as defined by *Naik et al*. [2005]) anthropogenic CH_4 emissions (97 Tg yr^{-1}; excluding agricultural waste burning) to zero. In the other simulation (RGLOB), we obtain the same 97 Tg yr^{-1} reduction by uniformly decreasing CH_4 emissions from all anthropogenic sectors (except for agricultural waste burning) by 39%. The decrease of 97 Tg yr^{-1} corresponds to an 18% reduction in total global CH_4 emissions.

The model includes the major CH_4 loss mechanism of reaction with tropospheric OH (450-480 Tg yr^{-1} in BASE; range reflects variability over the 15 years), as well as minor losses to soils (20 Tg yr^{-1} in BASE, imposed via a deposition velocity) and in the stratosphere (50-70 Tg yr^{-1} in BASE). Methane losses in the stratosphere by reaction with OH and $O(^1D)$ are modeled explicitly, and loss by reaction with chlorine is accounted for by prescribing the CH_4 concentration in the upper two model levels (above 14 hPa) to zonally and monthly averaged values from the middle atmosphere model Study of Transport and Chemical Reactions in the Stratosphere (STARS) [*Brasseur et al*., 1997] as described by *Horowitz et al*. [2003]. For the 30-year RGLOB simulation, these climatological values were decreased by 18% in an effort to account for the decrease in stratospheric concentrations that would result from the reduction in CH_4 emissions.

Emissions of O_3 precursors besides CH_4 from all sources are as described by *Horowitz et al*. [2003] except for NO_x emissions from ships, which have been removed on the basis that their inclusion likely leads to unrealistically high NO_x concentrations in the marine boundary layer in global models that neglect the rapid NO_x destruction recently observed to occur inside the ship plume [*Kasibhatla et al*., 2000; *Chen et al*., 2005]. *Eyring et al*. [2007], however, found that the ensemble mean oceanic NO_x concentrations from 10 global models that included ship emissions fell within the range of a wider observational dataset than that used by *Kasibhatla et al*. [2000]. They point out, however, that the modeled difference from including versus excluding ship emissions is too weak to be accurately evaluated with available measurements [*Eyring et al*., 2007]. While the impact of ship NO_x emissions on the oceanic atmosphere is still uncertain, *Eyring et al*. [2007] show that the ship NO_x emissions in the year 2000 CLE inventory (which we include in our transient future scenarios described below) decrease the CH_4 lifetime in the models by 0.13 years (10-model ensemble mean). We further discuss the impact of ship NO_x emissions in the context of our results in Section 4.

2.2 Transient Future Scenarios

In order to project the impact of CH_4 emission controls on future air quality and climate, we conduct a second set of transient simulations, using the "Current Legislation" (CLE) scenario for 2000 to 2030 as a baseline [*Cofala et al*., 2005; *Dentener et al.*,

2005]. This scenario incorporates existing emission control legislation on the traditional air pollutants NO_x, CO, and NMVOC around the globe to describe the evolution of O_3 precursors [*Dentener et al*., 2005] and is thus more optimistic than the widely used IPCC SRES scenarios [*Nakicenovic et al*., 2000]. Simulations applying 2000 and 2030 CLE emissions, but with uniform CH_4 abundances, were previously conducted with MOZART-2 and analyzed as part of the multi-model ACCENT Photocomp Experiment 2 [*Dentener et al*., 2006ab, *Shindell et al*., 2006, *Stevenson et al.*, 2006, *van Noije et al*., 2006].

Here, we conduct transient simulations for 2000-2030 following the CLE scenario, with the period 2000-2004 used for spin-up. We adopt the approach of *Dentener et al*. [2005], interpolating the CLE emissions provided for the years 2000, 2010, 2020, and 2030 to obtain annual emissions; Table 2 shows the growth of CH_4 emissions from 2005 to 2030. Between 2005 and 2030, baseline CLE anthropogenic emissions of CH_4, NO_x, CO, and NMVOC change by +29% (+96 Tg CH_4 yr^{-1}), +19% (+5.3 Tg N yr^{-1}), -10% (-44 Tg CO yr^{-1}), and +3% (+3 Tg C yr^{-1}), respectively. Aircraft emissions are assumed to grow linearly, from 0.8 to 1.7 Tg N yr^{-1} (NO_x) and 1.7 to 3.7 Tg yr^{-1} CO, as recommended for the ACCENT Photocomp Experiment 2 simulations for 2000 and 2030 [*Stevenson et al*., 2006], based on the IS92a scenario [*Henderson et al*., 1999]. Biomass burning emissions are taken from the 1997-2002 GFED v.1 biomass burning climatology [*van der Werf et al*., 2003], vertically distributed following the recommendations for the ACCENT Photocomp Experiment 2, and assumed constant into the future. Wetland emissions are based upon the seasonal and spatial distribution from *Wang et al*. [2004] as described by *Fiore et al*. [2006], but here we reduce CH_4 emissions from swamps by 12 Tg yr^{-1}, in an effort to reduce the positive tropical bias as compared to the NOAA GMD observations found in that study. The NCEP meteorology for 2000-2004 is recycled every 5 years to allow for interannual variability in the O_3 response to CH_4; these years were chosen on the basis of our previous work showing that the meteorology during these years yields a relatively constant CH_4 lifetime when emissions are held constant [*Fiore et al*., 2006], and thus should minimize discontinuous changes in the CH_4 sink by tropospheric OH when the winds are recycled. Losses of CH_4 transported into the stratosphere are treated as described in Section 2.1 with the exception

of the prescribed climatology in the upper 2 model levels; we instead relax the model CH_4 concentrations in these levels to zero with a six month lifetime to account for CH_4 loss by reaction with chlorine. The six month lifetime retains the same present-day stratospheric loss rate as in BASE, while allowing the stratospheric CH_4 sink to adjust to changes in the atmospheric burden resulting from changes in emissions. Additional model updates in these simulations include an increase of the $O(^1D) + N_2$ rate constant [*Ravishankara et al*., 2002] and the inclusion of near-infrared photolysis of HO_2NO_2 [*Roehl et al*., 2002].

We conduct three simulations using CH_4 reduction scenarios relative to the baseline CLE scenario beginning in 2006 (Figure 2). Compared to the 17% increase in total CH_4 emissions in the baseline CLE scenario between 2005 and 2030 (Table 2), emissions increase by only 4% in scenario A and decline by 5% and 15% in scenarios B and C, respectively, over this period. Further details on the development of these scenarios are provided by *West et al*. [2007b], along with an estimate of the associated costs and public health benefits. Briefly, scenario A corresponds to an 18% (75 Tg yr^{-1}) decrease in global anthropogenic CH_4 emissions (defined as the agricultural and industrial sectors provided in the CLE inventory) relative to the projected CLE emissions in 2030. Scenario B involves a 29% (125 Tg yr^{-1}) decrease in global anthropogenic CH_4 emissions in 2030, slightly less than the reductions achieved in the IIASA Maximum Feasible Reductions (MFR) scenario versus CLE in 2030, and should be cost-effective with available technologies at a marginal cost of approximately $315 per ton CH_4 ($15 per ton CO_2 equivalent). Scenario C requires development of additional control technologies, likely in the large agricultural sector, to achieve a 42% (180 Tg yr^{-1}) reduction of global anthropogenic CH_4 emissions by 2030.

2.3 Steady-State Simulations

We conduct four "steady-state" simulations to diagnose the relative contribution to surface O_3 from CH_4 oxidation in the free troposphere versus boundary layer (Table 1). In these simulations, we use the BASE emissions for all species besides CH_4, but fix atmospheric CH_4 mixing ratios to (1) 1760 ppb everywhere (GLOB1760 simulation), (2) 1460 ppb everywhere (GLOB1460), (3) 1460 ppb in the boundary layer and 1760 ppb

elsewhere (PBL1460) , and (4) 1760 ppb in the boundary layer and 1460 ppb elsewhere in the free troposphere (FT1460). The model level centered at 750 hPa (top edge at 724 hPa or ~2.5 km) is included as the uppermost level within the boundary layer. These four simulations were spun up beginning in May 1999 and results are examined for the year 2000. We conduct an additional simulation in which we use the CLE 2030 emissions for non-CH_4 O_3 precursors and fix CH_4 concentrations uniformly to the 700 ppb pre-industrial level, in order to quantify the total contribution of anthropogenic CH_4 to tropospheric O_3 in the year 2030.

2.4 Model Evaluation

The annual mean latitudinal bias in our CH_4 simulations (BASE and CLE) is compared to the NOAA GMD observations [*Dlugokencky et al*., 2005] for the year 2004 in Figure 3. For both simulations, the simulated CH_4 concentrations are within 5% of the observations at all locations. The BASE simulation has previously been shown to capture much of the observed CH_4 rise in the early 1990s, along with the flattening in the late 1990s [*Fiore et al*., 2006]. A major shortcoming in BASE is the 50% overestimate of the mean 2004 gradient from the South Pole to Alert (195 ppb vs. 127 ppb observed). This overestimate is corrected in the CLE simulation (121 ppb gradient) largely due to the use of the *Wang et al*. [2004] wetland distribution, which also improves the seasonal cycles in the model at northern hemispheric sites [*Fiore et al*., 2006]. As we show in Section 4, the O_3 response to CH_4 emission reductions is insensitive to biases in the simulated CH_4 distribution.

Global distributions of O_3 and its precursors in a different version of MOZART-2 were evaluated with available observations by *Horowitz et al*. [2003] who showed that the model generally captures the observed O_3 seasonality, as well as horizontal and vertical gradients. On the regional scale, however, *Murazaki and Hess* [2006] previously showed a >20 ppb mean bias in the MOZART-2 simulation of surface O_3 as compared to the EPA AIRS monitoring sites over the eastern United States in summer. Our updated treatment of isoprene nitrates decreases simulated July afternoon surface O_3 concentrations by 4-12 ppb over the eastern United States [*Fiore et al*., 2005]. We note that the surface O_3 sensitivity to CH_4 does not appear to be strongly influenced by the

remaining bias as our results below are consistent with the sensitivity previously diagnosed by the GEOS-Chem model, which exhibits a smaller bias compared to U.S. surface O_3 observations [*Fiore et al*., 2002ab; *Fiore et al*., 2005].

Most pertinent to our study is the ability of the model to represent the global distribution of NO_x. *Horowitz et al*. [2003] showed that the model typically fell within the observed range of NO_x concentrations throughout most of the troposphere. The largest discrepancies in NO_x concentrations occurred in surface air near islands, where the model overestimates measurements of clean marine boundary layer air due to mixing of emissions throughout the coarse-resolution grid cell [*Horowitz et al*., 2003]. When we compare our CLE and BASE NO_x simulations for the meteorological year 2004 with the *Horowitz et al*. [2003] simulation, we find that the NO_x distributions are similar in most regions of the globe (not shown). The largest difference is found in the upper troposphere (beginning about 5-7 km), mainly in the tropical Pacific (*e.g*. over Christmas Island, Tahiti, Guam, the Philippine Sea) and in the southern Atlantic, where NO_x concentrations in our simulations are often lower than those in *Horowitz et al*. [2003] (and the observations) by a factor of two or more. This result likely reflects differences in the lightning NO_x distribution which is driven by the NCEP reanalysis in our simulations but by the NCAR MACCM3 meteorology in *Horowitz et al*. [2003]. In the ACCENT Photocomp Experiment 2, MOZART-2 NO_2 columns (in a simulation using year 2000 CLE emissions and CH_4 concentrations set to 1760 ppb) were consistently 10-30% higher than the model ensemble mean [*van Noije et al*., 2006]. The comparison with NO_2 columns retrieved from the GOME instrument using three different methods varied widely, however, with MOZART-2 falling below the retrieved range in the Eastern U.S. (-3%), Eastern China (-15%) and South Africa (-48%); within the range in Europe and Northern Africa, and exceeding the range in Central Africa (+7%), South America (+39%), and Southeast Asia (+6%) [*van Noije et al*., 2006].

2.5 Distribution of CH_4 loss and O_3 production in the BASE simulation

We examine the latitudinal and vertical distributions of CH_4 and tropospheric O_3 production in the BASE simulation, focusing here on the final year of the 30-year simulation. The strong temperature dependence of the CH_4-OH reaction largely restricts

CH_4 oxidation to the lower troposphere. Following the approach recommended by *Lawrence et al*. [2001], we find that 57% and 90% of the CH_4 loss by reaction with OH occurs below 750 and 500 hPa, respectively (Table 3). This estimate is somewhat higher than previous work estimating that CH_4 oxidation below 500 hPa accounts for ~80% of the CH_4 loss [*Spivakovsky et al*., 2000; *Lawrence et al*., 2001]. While it is possible that OH in MOZART-2 may be larger in the lower troposphere than in previous modeling studies, the CH_4 lifetime against tropospheric OH is 10.3 years, within the range of other models (8.2-11.7 years based on *Stevenson et al*. [2006]). Most of the CH_4 loss (75%) occurs in the tropics, consistent with the estimate by *Spivakovsky et al*. [2000] of 78% of CH_4 loss between 32°S and 32°N. Table 3 also shows a hemispheric asymmetry, with nearly twice as much CH_4 loss occurring north of 30°N than south of 30°S, and 20% more loss in the northern tropics than in the southern tropics. Since the CH_4 burden is evenly distributed (<4% difference between the hemispheres), the asymmetry in the CH_4 chemical loss reflects the OH distribution (Figure 4a), which in turn is governed by the larger NO_x emissions and resulting NO_x abundances in the northern hemisphere (Figure 4b). Ozone production in the model is also larger in the northern hemisphere, where shorter-lived anthropogenic O_3 precursors are most abundant (*e.g.* NO_x in Figure 4b), contributing ~60% to the total global production, consistent with the estimate from *Horowitz et al*. [2003]. Our BASE simulation predicts a slightly larger contribution from lower tropospheric O_3 production than in *Horowitz et al*. [2003] (51% vs. 46%).

3. Linearity of global annual mean O_3 response to CH_4 controls

Figure 5 shows that the decreases in tropospheric CH_4 and O_3 from sustained CH_4 emission reductions (RGLOB-BASE) are approaching a steady state after 30 years of simulation. We use the final year of the simulations to diagnose the model "feedback factor", the ratio of the perturbation lifetime (*PT*; the decay time for a perturbation such as a pulse of CH_4 emissions) to the total atmospheric lifetime ($LT = B/L_{CH4}$): $PT/LT = 1/(1-s)$ where B is the total atmospheric CH_4 burden, L_{CH4} is the total atmospheric CH_4 loss, and $s = \delta \ln LT / \delta \ln B$ [*Prather et al*., 2001]. We use the difference in lifetimes and burdens between the RGLOB and BASE simulations to calculate $s = 0.23$, corresponding to $PT/LT = 1.30$, somewhat smaller than the model range of 1.33-1.45

reported by *Prather et al.* [2001]. In the BASE simulation, LT = 8.7 years, equal to the mean of the range reported for current CTMs (8.7±1.3 years) [*Stevenson et al.*, 2006]. We thus obtain a CH_4 perturbation time of 11.3 years and estimate that the model results in year 30 capture 93% ($1-e^{-30/11.3}$) of the steady-state change, ultimately yielding a 23% steady-state decrease in atmospheric CH_4 (1090 Tg CH_4 or 400 ppb surface mixing ratio) from the 18% decrease in total CH_4 emissions in RGLOB.

We scale the tropospheric O_3 burden and surface O_3 responses (RGLOB-BASE) in year 30 to obtain ultimate steady-state decreases of 10.3 Tg tropospheric O_3 (blue filled circle in Figure 1) and 1.0 ppb surface O_3 (global annual mean). The sensitivity of 0.11 Tg O_3 (or 11 ppt surface O_3) decrease per Tg CH_4 yr^{-1} emission reduction diagnosed from these simulations is slightly lower than the 0.12-0.16 Tg O_3 range of the prior work displayed in Figure 1. In particular, the results of *Shindell et al.* [2005] (green squares in Figure 1) yield a larger sensitivity of ~0.16 Tg O_3 per Tg CH_4 yr^{-1} emission.

Annual mean results from the transient future scenarios (Section 2.2) are shown in Figure 2. With the more aggressive controls in scenarios B and C, CH_4 concentrations decrease by 2030 to levels last observed in the 1990s and 1980s, respectively (Figure 2b). The tropospheric O_3 burden increases from 2005 to 2030 under all scenarios, by 17.0, 12.3, 7.7, and 2.8 Tg for scenarios CLE, A, B, and C, respectively (Figure 2c), reflecting the 19% growth in anthropogenic NO_x emissions. The global annual mean 8-hour daily maximum (MDA8) surface O_3 increases by 1.8 ppb in the baseline CLE scenario. The CH_4 control scenarios counteract some of this increase in surface O_3, with the most aggressive CH_4 controls (scenario C) almost entirely offsetting this increase (total change of +0.2 ppb from 2005 to 2030; Figure 2d). Figures 2c and 2d illustrate the effect of interannual variability in meteorology on tropospheric O_3, as evidenced by the repeating 5-year cycle superimposed upon the longer-term trend. This variability likely reflects year-to-year variations in lightning NO_x emissions (which vary from 3.1-3.4 Tg N yr^{-1}) and/or exchange with the stratosphere (varies from 850-880 Tg yr^{-1}), both of which correlate strongly with annual mean tropospheric O_3 burdens in the BASE simulation with 1990-2004 meteorology (r^2 = 0.80 and 0.92, respectively, for the first 15 year period).

Although not at steady state, the results in Figure 2 scale approximately linearly to the emission changes, despite differences in the trajectory shapes of the emission controls over the 25 years. By comparing results for 2030 in scenarios A, B, and C with those from the baseline CLE simulation, we obtain a range of 0.06 (scenario A) to 0.08 (scenario C) Tg O_3 decrease per Tg CH_4 yr^{-1} reduced. These values are lower than that from the RGLOB simulation since the CLE, A, B, and C simulations have not yet reached a steady state. The larger sensitivity implied by scenario C reflects the deeper CH_4 reductions that are imposed earlier in this emission control trajectory (Figure 2a), allowing for a relatively larger O_3 burden change to be realized by 2030. In an attempt to remove the influence of the shapes of the trajectories in Figure 2a on the results, we assume that the *PT* of 11.3 years diagnosed from RGLOB-BASE applies for the future scenarios (it may in fact differ since a different base emission inventory is used, which will influence OH). We then define an "effective CH_4 emission control" in the year 2030 ($\Delta E_{eff\text{-}2030}$) to represent the change in CH_4 emissions that would produce a steady-state response equal to the transient response in 2030 in each of our simulations (which are not at steady state). The $\Delta E_{eff\text{-}2030}$ is calculated as the sum of the emission controls applied in each year from 2005 to 2030, weighted by the fraction of the steady-state response that should be realized by 2030. In this manner, we estimate that $\Delta E_{eff\text{-}2030}$ is -35, -76, and -117 Tg CH_4 yr^{-1} for scenarios A, B, and C, respectively, corresponding to a realization of 47%, 61%, and 65% of the total CH_4 emission reductions by 2030. Using the $\Delta E_{eff\text{-}2030}$, we estimate revised sensitivities of 0.14, 0.12, and 0.12 Tg O_3 decrease per Tg CH_4 yr^{-1} "effective" emission reductions, in good agreement with the 0.12-0.16 range of the published results displayed in Figure 1, but slightly higher than the sensitivities obtained above from RGLOB-BASE. Finally, we use these sensitivities to obtain steady-state changes in the O_3 burden of 10.1, 15.3, and 21.8 Tg for constant emissions at 2030 levels in scenarios A, B, and C, which we show in Figure 1. An alternative approach to diagnose $\Delta E_{eff\text{-}2030}$ is to consider the change in the CH_4 loss rate between the perturbation and baseline scenarios. With this approach, we estimate $\Delta E_{eff\text{-}2030}$ of -44, -86, and -130 Tg CH_4 yr^{-1} for A, B, and C, respectively, which translate to sensitivities of 0.11 Tg O_3 decrease per Tg CH_4 yr^{-1} reduced, equivalent to that in RGLOB-BASE, and within 11-26% of the results obtained via the former approach.

We next estimate the total contribution of anthropogenic CH_4 emissions to tropospheric and surface O_3 by comparing our CH_4-700 and CLE baseline simulations in 2030. The CH_4 loss by OH in the CH_4-700 simulation is 240 Tg CH_4 yr^{-1}. Using the lifetimes from *Prather et al.* [2001] for CH_4 loss to the stratosphere (120 years) and to soils (160 years), we estimate the total CH_4 loss (equal to the implied emissions) to be 270 Tg CH_4 yr^{-1}. The implied emissions are thus within 10% of the 245 Tg CH_4 yr^{-1} natural plus biomass burning emissions in the baseline scenario (Table 2), indicating that this simulation can be used to estimate the impacts of setting 2030 anthropogenic CH_4 emissions to zero. We note that zero anthropogenic CH_4 could not possibly be achieved by 2030 even if anthropogenic emissions were shut off instantly in 2005, since some anthropogenic CH_4 would still remain in the 2030 atmosphere (~11% for a *PT* of 11.3 years). We find that anthropogenic CH_4 contributes 40 Tg to the tropospheric O_3 burden and 4 ppb to global annual mean surface concentrations in 2030. For comparison with the other simulations in Figure 1, we calculate the $\Delta E_{eff\text{-}2030}$ for the baseline CLE scenario (+63 Tg CH_4 yr^{-1}), to estimate the steady-state increase of +26 Tg in the O_3 burden. Relative to the steady-state CLE value, the CH_4-700 simulation yields a decrease of 49 Tg O_3 (included in Figure 1) or a sensitivity of 0.11 Tg tropospheric O_3 (11 ppt surface O_3) per Tg CH_4 yr^{-1} effective emission change, consistent with that diagnosed above from RGLOB-BASE.

The similarity in the steady-state O_3 response to CH_4 in our simulations and in the published literature implies that the CH_4 and O_3 changes resulting from perturbations to CH_4 emissions can be accurately approximated, even when other OH precursors are evolving, by scaling to the effective CH_4 emission change relative to the baseline CH_4 emission scenario. Multiple computationally expensive transient simulations should only be needed in situations where OH changes substantially, as would be expected if CH_4 emissions doubled [*Prather,* 1996]. In most cases, one steady-state simulation relative to the baseline scenario should be sufficient to determine the model sensitivity of O_3 (and its spatial distribution; see Section 4) to CH_4. For estimating changes in global annual mean O_3, results can be approximated to within ~30% without using a model, given the range of 0.11-0.16 Tg O_3 burden or 11-15 ppt surface O_3 per Tg yr^{-1} change in CH_4 emission diagnosed from our simulations and the prior modeling studies in Figure 1.

4. Spatial distribution of the O_3 response to changes in CH_4 emissions

When anthropogenic CH_4 emissions are reduced (in the RGLOB vs. BASE simulations), gross O_3 production and O_3 concentrations decrease everywhere (Table 3 and Figure 6a), with the largest percentage changes occurring in the southern hemisphere (Figure 6b) where CH_4 contributes to a larger fraction of the O_3 production (since NMVOC abundances are lower than in the northern hemisphere). Annual mean O_3 concentrations decrease by 0.5-2.0 ppb throughout the troposphere (Figure 6a), with the largest decreases centered around 30°N where OH and NO_x are enhanced in the lower troposphere compared to other latitudes (Figure 4). *West and Fiore* [2005] previously noted an enhanced response of surface O_3 to CH_4 decreases centered around 30°N and suggested that it reflects O_3 production from CH_4 in the free troposphere at these latitudes where NO_x is abundant, followed by downwelling of that air to the surface, a hypothesis that we examine further in Section 5.

We plot in Figure 7 the tropospheric O_3 columns, relevant for climate forcing, as well as MDA8 O_3 concentrations in surface air, an indicator of air quality, in the BASE simulation. The highest annual mean tropospheric O_3 columns and MDA8 surface O_3 levels occur in the northern hemisphere over and downwind of continental regions where anthropogenic emissions of O_3 precursors are largest (Figures 7a and 7e). Figure 7 also shows the O_3 response to CH_4 emission changes, which exhibits considerable spatial structure.

Similar patterns of decreases in tropospheric O_3 columns in response to CH_4 controls occur in the RGLOB (Figure 7b) and scenario B (Figure 7c) simulations ($r = 0.98$). While maximum O_3 decreases are centered at 30°N (as in Figure 6a), large decreases in tropospheric O_3 columns also extend southward into the tropical Atlantic ocean and Africa. Figures 7f and 7g show broadly similar patterns in the decreases of annual mean MDA8 surface O_3 from CH_4 controls, but the correlation is weaker than for the tropospheric O_3 columns ($r = 0.88$). Figure 7f indicates that the largest benefits to air quality should occur over land, whereas the maximum decreases in surface O_3 in Figures 7g and 7h are over the Gulf of Mexico, North Atlantic, and extend eastward across northern Africa and the Middle East into the Arabian Sea and Bay of Bengal. These

discrepancies stem from differences in the NO_x emissions in the BASE and CLE inventories. For example, the model predicts a strong enhancement of O_3 production (and a strong sensitivity to CH_4) in NO_x-saturated ship track plumes in the CLE scenario, which does not occur in the sustained CH_4 reduction scenarios where ship NO_x emissions were excluded (Section 2.1). The dispersion of ship NO_x emissions into a coarse model grid box likely results in an artificially high O_3 production efficiency [*Kasibhatla et al.*, 2000; *Liang and Jacobson*, 2000] and we thus expect that the sensitivity of O_3 to CH_4 oxidation is overstated in the ship tracks in Figure 7g and 7h. Nevertheless, this result highlights that the O_3 response to CH_4 depends strongly on NO_x; accurately representing the global NO_x distribution is thus important for simulating this sensitivity.

The geographical patterns of the O_3 response to CH_4 controls are identical among the future CH_4 control scenarios (A, B, C), implying that the O_3 response is determined by the distribution of the shorter-lived species OH and NO_x which govern the O_3 production from CH_4 oxidation. As such, we focus in Figure 7 and thereafter on results from scenario B, noting that the magnitude of the O_3 change scales linearly to the "effective CH_4 emission controls" defined in section 3.

Comparing the O_3 response in scenario B with that in the CH_4-700 simulation (third and fourth columns in Figure 7) illustrates that the O_3 response exhibits an identical spatial pattern in a full transient CH_4 simulation and in a simulation with CH_4 set to a globally uniform, fixed value (spatial correlation of r=1.0 between Figures 7c and 7d, and between Figures 7g and 7h). This result indicates that the O_3 response is insensitive to biases in the simulated CH_4 distribution. Furthermore, the linearity of the O_3 response to CH_4 (Figure 1 and Section 3) implies that the spatial pattern can be scaled to different magnitudes of CH_4 controls.

Finally, we examine the extent to which the spatial pattern of the surface O_3 response varies with changes in meteorology in the final 15 years of our sustained CH_4 reduction simulations (RGLOB-BASE). The interannual variability is <5% in most world regions, except for in the tropics, on the west coast of central South America, and off the southwestern coast of United States where it is 10-20% (not shown). We conclude that the spatial patterns in Figure 7 are fairly robust to fluctuations in present-day meteorology.

5. Surface O_3 contribution from CH_4 oxidation in the free troposphere vs. boundary layer

Surface O_3 is influenced by CH_4 oxidation both within the boundary layer and in the free troposphere (followed by subsidence of this air to the surface). With our steady-state simulations (Section 2.3), we separate the contributions to surface O_3 from CH_4 oxidation in these two regions. We focus our analysis on the PBL1460 and FT1460 simulations relative to GLOB1760 since we find our results to be linear; the O_3 response to reductions of CH_4 throughout the atmosphere (GLOB1460-GLOB1760) are virtually identical to the sum of the O_3 changes from reducing CH_4 in the boundary layer (PBL1460-GLOB1760) and from reducing CH_4 in the free troposphere (FT1460-GLOB1760).

At nearly all surface locations, oxidation of CH_4 in the boundary layer contributes more than 50% of the change in annual mean MDA8 O_3 resulting from CH_4 controls (Figure 8), with a global mean contribution of 64%. The 300 ppb decrease in boundary layer CH_4 concentrations decreases MDA8 O_3 in surface air by up to 1 ppb O_3 in the NO_x-rich regions of the northern mid-latitudes and in southern Africa (Figure 8a). Surface O_3 is also decreased by the reduction in CH_4 oxidation in the free troposphere near the downwelling branches of the Hadley cell, at roughly 30°N and 30°S, particularly over the Sahara region of North Africa, the Middle East, and the Caribbean Sea where the 300 ppb decrease in free tropospheric CH_4 concentrations lowers surface O_3 by ~0.5 ppb (Figure 8b).

As a case study, we plot the composite maximum MDA8 O_3 decrease over the United States resulting from a 300 ppb decrease in CH_4 in the planetary boundary layer (below 724 hPa; PBL1460-GLOB1760) in Figure 9. Southern California and the New York – New Jersey region in the northeastern United States exhibit a larger peak O_3 decrease (> 2-3 ppb) from the CH_4 reduction than the rest of the country. In these NO_x-saturated regions, CH_4 oxidation within the planetary boundary layer accounts for 70-80% of the total O_3 decrease from CH_4 reductions (Figure 8c). We conclude that the surface O_3 response to CH_4 is strongly enhanced in locations with NO_x-saturated chemistry, and weakly enhanced in regions of downwelling air.

The question arises as to whether our coarse resolution global model accurately represents the response of O_3 to CH_4 at the urban scale. Higher-resolution model calculations of O_3 production in urban airsheds support the conclusion that O_3 production in polluted urban areas is sensitive to CH_4. For example, it has been estimated that despite its low reactivity, CH_4 oxidation contributes approximately 10-20% of the O_3 formed downwind of London in the urban plume [*Hough and Derwent*, 1987; *Derwent et al*., 1991]. *Martien and Harley* [2006] used adjoint methods to identify a strong VOC-sensitivity in and downwind of core urban areas. The consistency of our global model results with the conclusions from these studies implies that the global model is useful in assessing the qualitative O_3 response to CH_4 in urban areas, although the accuracy of the results for a particular urban core will depend upon the model representation of the VOC-NO_x sensitivity.

6. Sensitivity of tropospheric O_3 to the location of CH_4 emissions

Given the long lifetime of CH_4, the O_3 produced from CH_4 oxidation is expected to be independent of the location of the CH_4 emissions. Instead, the spatial pattern of the O_3 from CH_4 oxidation should be controlled by the distributions of OH and NO_x, which have much shorter lifetimes and affect both the location of the CH_4 oxidation and the amount of O_3 produced per CH_4 molecule oxidized. We directly test this assumption by comparing the results from the RASIA simulation, in which Asian anthropogenic CH_4 emissions are set to zero, with those from the RGLOB simulation, in which an equivalent CH_4 emission reduction was distributed globally.

Figure 10 compares the MDA8 surface O_3 in RASIA and RGLOB simulations in year 11 (note that The RASIA simulation was stopped after 11 years since there was little difference in the O_3 response from that in RGLOB). Except for the immediate source region over Asia, there is <10% difference in other northern hemispheric source regions, <5% difference over the rest of the northern hemisphere, and <1% difference in the southern hemisphere. Annual mean tropospheric O_3 columns in year 11 are even more similar between the simulations (<0.5% differences; not shown). These results imply that control options could be targeted starting with the least-cost reductions available

anywhere in the world since the global air quality and climate benefits of CH_4 controls do not depend strongly upon the location of the emission reductions.

7. Regional air quality

We first investigate the seasonality of the regional surface O_3 response to CH_4 using the simulations with sustained CH_4 reductions (RGLOB-BASE; Figure 11). Both Europe and South Asia show some seasonal variation (0.8 and 0.5 ppb amplitude, respectively) whereas there is little seasonality over the United States, East Asia and Africa. These results are consistent with the findings from a multi-model intercomparison of the surface O_3 response to a 20% decrease in global CH_4 mixing ratios, although the regional definitions in that study are not identical [*TF HTAP*, 2007]. The enhanced response over Europe in summertime and over South Asia in April may reflect a more NO_x-saturated O_3 formation regime than during the peak O_3 seasons in the United States and Africa, where biogenic VOC are more abundant.

Next, we examine the percentage of model grid box-days where MDA8 $O_3 \geq$ 70 ppb in surface air (a metric for polluted conditions) by season for the selected world regions in the future scenarios. Figure 12 shows that air quality degrades substantially under the baseline CLE scenario from 2005 to 2030 in South Asia, where large growth in emissions (+58% for NO_x) from the transport and power generation sectors is projected [*Dentener et al*., 2005]. From 2005 to 2030, the percentage of model grid cell-days with MDA8 $O_3 \geq 70$ ppb increases by 4%, 1%, and 2% in the United States, Europe, and Africa, respectively, during summer, the season in which high-O_3 events peak for those regions (Figure 12). Peak incidences occur in spring in the Asian regions, with increases of 4% (for East Asia) and 14% (for South Asia) in the percentage of model grid cell-days with MDA8 $O_3 \geq 70$ ppb from 2005 to 2030. These findings are consistent with prior modeling studies in which the CLE scenario produced surface O_3 increases of ~10 ppb over the Indian subcontinent from 2000 to 2030, and of ~2 ppb globally, with little change over some regions of North America, Europe and Asia [*Dentener et al*., 2006b; *Stevenson et al*., 2006].

We evaluate here the ability of the global model to represent the threshold statistic presented in Figure 12, and determine whether those results can be extended to other

thresholds. A similar statistic was previously used by *Fiore et al*. [2002a] who found that a global model was able to simulate adequately the percentage of total grid box-days above 70 ppb in the United States during the summer of 1995 (observed values of 5%, 15% and 36% for thresholds of 80, 70, and 60 ppb and simulated values of 1%, 10%, and 37%). In our CLE simulation for 2005, we find that 5%, 13% and 26% of grid box-days over the United States in summer exceed 80, 70, and 60 ppb thresholds, respectively. We further find that the changes due to CH_4 emission controls are relatively insensitive to the chosen threshold, such that in 2030, scenario A yields a ~5% decrease in the incidence of grid box-days above 60, 70, and 80 ppb relative to the CLE scenario. For scenarios B, C, and CH_4-700, the corresponding percentage changes are ~10%, ~15%, and ~35%. Below, we focus on results for the 70 ppb threshold.

All of our CH_4 reduction scenarios decrease the percentage of model grid cell-days with MDA8 $O_3 \geq 70$ ppb in 2030, by up to 3% (Europe) to 12% (South Asia) when all anthropogenic CH_4 is removed (Figure 12). The cost-effective CH_4 reductions in scenario B yield percentage decreases of 1%, 1%, and 2% in Africa, Europe, and the United States in summer, and of 3% in both Asian regions in spring compared to CLE. For all regions, the largest decreases in the percentage of high-O_3 events occurs in the same season as the peak number of model grid cell-days with MDA8 $O_3 \geq 70$ ppb, except for the United States where the decrease is slightly larger in spring.

During summer in Europe and fall in East Asia, aggressive CH_4 controls (scenarios B and C) would decrease high-O_3 events to below 2005 levels. For the United States and Africa, only the CH_4-700 simulation reduces high-O_3 events below the 2005 levels. The dramatic growth of O_3 precursor emissions over South Asia leads to additional model grid-cell days where MDA8 $O_3 \geq 70$ ppb, even with the drastic reduction of CH_4 to pre-industrial levels.

In Figure 13, we assess the potential for CH_4 controls to reduce MDA8 O_3 in surface air under background, average, and highly polluted conditions. We focus on the high-O_3 season for each region, when the incidence of grid-square days ≥ 70 ppb is maximum in the year 2030, and plot the distribution of the change in MDA8 surface O_3 in response to the CH_4 controls in scenario B (B-CLE), as a function of the MDA8 O_3 values in the baseline CLE simulation for the year 2030. Within the United States,

results are shown for the four quadrants in order to illustrate differences that can occur within large continental-scale regions.

The median O_3 decrease tends to grow linearly to a maximum of ~2 ppb at CLE 2030 MDA8 O_3 concentrations of 60-90 ppb (Figure 13). In contrast, the median response in the western U.S. quadrants increases linearly over the entire O_3 distribution, with days when total O_3 > 90 ppb nearly always associated with decreases of >1 ppb and >2.5 ppb for the northwestern and southwestern quadrants, respectively; these conditions are typically associated with boundary layer stagnation and the strong O_3 response reflects the relatively high sensitivity to CH_4 oxidation in the polluted boundary layer in southern California (Figures 8 and 9). In Figure 13, O_3 also exhibits a strong sensitivity to CH_4 on the most polluted grid-cell days (>90 ppb) in Europe, East Asia, and Africa, often decreasing by >1ppb under scenario B.

The median response in the southeastern U.S. quadrant peaks at ~40 ppb total O_3 and then weakens as total O_3 increases further. This feature reflects the meteorology in the southeastern U.S. in summer. The cleanest conditions are associated with inflow of marine air from the Gulf of Mexico; the stronger median sensitivity at 10-40 ppb total O_3 over the southeastern U.S. compared to the other U.S. regions in Figure 13, stems from the enhanced contribution of CH_4 oxidation in the free troposphere (followed by mixing into the boundary layer) over the Gulf of Mexico (Figure 8). The most polluted conditions are associated with stagnation events that suppress mixing between the free troposphere and boundary layer [*Logan,* 1989; *Eder et al*., 1993; *Jacob et al*., 1993]. Given that O_3 chemistry over the southeastern United States is NO_x-sensitive due to abundant biogenic VOC emissions [*Chameides et al*., 1988], CH_4 contributes less to O_3 on the most polluted days than in the NO_x-saturated regions of the western and northeastern United States.

Peak decreases of ≥ 4 ppb (indicated by the lower extent of the vertical lines in Figure 13) occur near the center of the overall distribution, within the range of 40-60 ppb for Europe; 20-70 ppb for Africa; 40-70 ppb for East Asia, 30-60 ppb for South Asia, and 30-100 ppb in the United States. Emissions of NO_x, CO, and NMVOC emissions on foreign continents were previously shown to exert a maximum influence on U.S. surface O_3 near the middle of the total O_3 distribution, under conditions of strong mixing with the

free troposphere [*e.g. Fiore et al.*, 2002b; *Li et al.*, 2002]. Similarly, the highest U.S. background O_3 concentrations (estimated in simulations where North American anthropogenic emissions of NO_x, CO, and NMVOC were turned off but O_3 generated from CH_4 oxidation was included) were found at the center of the overall surface O_3 distribution and attributed to O_3 mixing down from the free troposphere [*Fiore et al.*, 2003]. The qualitative similarity of the results in Figure 13 to prior studies provides some confidence that our findings are robust to the model bias in surface O_3 (Section 2.4) although we cannot rule out some influence of the bias on the quantitative results, particularly at the high tail of the O_3 distribution.

We conclude that the scatter in the MDA8 O_3 changes in Figure 13 likely reflects differences in meteorology (mixing with the free troposphere versus local stagnation) as well as in chemistry (the local sensitivity of ozone production to CH_4). The smaller sensitivity to CH_4 at the low end of the total O_3 distribution reflects cleaner air and does not necessarily imply a lack of mixing between the boundary layer and the free troposphere. The larger than average response in the upper tail of the total O_3 distribution over most regions typically occurs under stagnant conditions and is driven by the local NO_x-saturated chemistry.

8. Climate Forcing

We estimate the radiative forcings from CH_4 and O_3 resulting from CH_4 emission reductions as a proxy for the climate response. For CH_4, we evaluate the analytical expression recommended by *Ramaswamy et al.* [2001], using the calculated global mean CH_4 concentrations to estimate the global mean adjusted forcing. Assuming a homogenous spatial distribution for CH_4 has been shown to introduce an error much less than 1% in radiative forcing relative to a calculation using a CH_4 distribution simulated by a CTM [*Ramaswamy et al.*, 2001]. The adjusted forcing from tropospheric O_3 is calculated with the GFDL AM2 radiative transfer model [*Freidenreich and Ramaswamy*, 1999; *Schwarzkopf and Ramaswamy*, 1999; GFDL GAMDT, 2004], with stratospheric temperature adjustment following the approach of *Naik et al.* [2007]. We caution that the spatial pattern of the temperature response will not generally follow that of the

radiative forcing [e.g. *Levy et al*., 2007], and a full climate model simulation would be needed to estimate the temperature response to the forcings shown here.

The global mean O_3 radiative forcing under the CLE baseline scenario (2030-2005) is 0.065 W m^{-2}, near the multi-model mean in the CLE scenario from 2000 to 2030 (0.063±0.015 W m^{-2}) reported by *Stevenson et al*. [2006]. The strongest forcing occurs in the tropics, particularly over South Asia and the Middle East regions (0.15-0.21 W m^{-2}) where the increases in tropospheric O_3 columns are largest (not shown). All of the CH_4 control scenarios yield a similar spatial pattern of decreases in O_3 forcing, with the largest decreases occurring broadly in the tropics and over the Middle East and northern Africa (Figure 14). The larger forcings in the tropics as compared to the poles reflect the spatial pattern of the change in tropospheric O_3 columns (Figure 7c) and the higher sensitivity of the forcing to the O_3 column at these latitudes (forcing efficiencies of 0.04-0.06 versus a global mean of 0.036 W m^{-2} DU^{-1}). Table 4 shows the global mean forcing from both CH_4 and O_3 for each 2030 sensitivity simulation. Aggressive CH_4 controls (scenarios B and C) would offset the positive net forcing from CH_4 and O_3 predicted to occur otherwise from 2005 to 2030 under the baseline CLE scenario. While the global mean forcing from CH_4 and O_3 roughly cancel in scenario B, we expect regional variations; for example, the positive forcing from O_3 may exceed the negative forcing from CH_4 in the tropics, with the opposite impact near the poles. Eliminating anthropogenic CH_4 emissions would reduce global mean radiative forcing from CH_4 and O_3 by 0.6 W m^{-2} relative to 2005 (by 0.7 W m^{-2} relative to the CLE 2030 baseline).

9. Conclusions

The potential to improve both climate and air quality by regulating CH_4 emissions has sparked discussion of CH_4 controls as a component of future air pollution policy [*EMEP*, 2005, *TF HTAP*, 2007]. Our analysis expands upon prior modeling studies [*Fiore et al*., 2002a; *Dentener et al.*, 2005; *West et al*., 2006, 2007a] to provide a basis for more fully assessing the monetary costs and benefits associated with managing global O_3 pollution by controlling CH_4 emissions [*West et al*., 2007b]. We employed two sets of full-chemistry multi-decadal transient simulations in the MOZART-2 global CTM to characterize the response of CH_4 and O_3 to changes in CH_4 emissions, and to estimate the

O_3 air quality and climate benefits that would result from CH_4 controls. We further diagnosed the relative impact of CH_4 oxidation in the free troposphere versus in the boundary layer on surface O_3, as well as the anthropogenic CH_4 contribution to tropospheric O_3, with a set of steady-state simulations.

Cost-effective future CH_4 controls through 2030 (our scenario B; <$315 per ton CH_4) would offset the projected positive climate forcing from CH_4 and O_3, and reduce the incidence of high surface O_3 events in all regions relative to the CLE baseline scenario; air quality would improve even relative to 2005 in Europe (summer and fall) and East Asia (fall). The mean O_3 decrease from CH_4 controls is often largest near the middle of the total O_3 distribution (*e.g.* ~40-70 ppb total O_3). Even during high-O_3 events, O_3 often decreases by >1 ppb in scenario B by 2030. Controlling CH_4 emissions could thus help to achieve compliance with air quality standards, particularly in situations where high-O_3 events are frequently within a few ppb of a threshold concentration, as is often the case in the United States.

Combining our results with estimates from the published literature, we find that global tropospheric O_3 decreases approximately linearly with reductions in CH_4 emissions: 0.11-0.16 Tg tropospheric O_3 or 11-15 ppt surface O_3 per Tg CH_4 yr^{-1}. This sensitivity implies a total contribution from present-day anthropogenic CH_4 emissions of ~50 Tg to the tropospheric O_3 burden and ~5 ppb to surface O_3. The similarity of the global mean sensitivity of O_3 to CH_4 in our simulations and those from other models shown in Figure 1, and of the spatial pattern in our transient and steady-state simulations (Figures 7c and 7g versus Figures 7d and 7h) indicates that the O_3 response to CH_4 is insensitive to biases in the simulated CH_4 distribution and thus to errors in the spatial distribution of emissions. We further expect that the sensitivity of O_3 to CH_4 in MOZART-2 is fairly robust to the positive surface O_3 bias versus observations over the eastern United States [*Fiore et al.*, 2005; *Murazaki and Hess*, 2006]), based on the consistency of our results with the other models in Figure 1, and of the results in Figures 12 and 13 with prior simulations with the GEOS-Chem model which has a much smaller bias compared to the observations [*Fiore et al*., 2002ab; *Fiore et al*., 2005].

We defined an "effective CH_4 emission change" to facilitate comparisons between transient and steady-state results. In the case of our future simulations, the effective CH_4

emission change in 2030 ($\Delta E_{eff\text{-}2030}$) is the sum of the emission controls applied in each year from 2005 to 2030, weighted by the fraction of the steady-state response that should be realized by 2030. We showed that once the relationship between $\Delta E_{eff\text{-}2030}$ and the resulting CH_4 concentration is established for a baseline scenario (in which emissions of NO_x and other OH precursors are evolving), the CH_4 and O_3 changes that would result from perturbing CH_4 emissions by a different magnitude relative to that scenario can be accurately approximated, eliminating the need for multiple computationally expensive transient simulations (as long as the OH is relatively constant). In many cases, one steady-state simulation relative to the baseline scenario should be sufficient to determine the model sensitivity of O_3 to CH_4, including the spatial distribution of the O_3 response. For estimating changes in annual global mean O_3, results can be approximated to within ~30% using the sensitivity estimated here, without needing additional model simulations.

The decreases in surface O_3 and tropospheric O_3 columns (relevant for air quality and climate, respectively) arising from CH_4 emission control are largely independent of source location, with the exception of ~10-20% enhancements in source regions. Although the surface O_3 response to CH_4 emission reductions is relatively homogenous across the globe compared with the response to controls on NO_x emissions [*West et al.*, 2007a], the decreases in surface O_3 are not uniform, reflecting a combination of local meteorological and chemical conditions.

We find in the model that global annual mean maximum daily 8-hour (MDA8) surface O_3 is nearly twice as sensitive to CH_4 in the planetary boundary layer (below ~2.5 km) than to CH_4 in the free troposphere. The surface O_3 response to CH_4 is strongly enhanced in locations with NO_x-saturated chemistry, including at the high tail of the O_3 distribution (*e.g.,* in southern California). Weaker enhancements occur in regions where surface air mixes frequently with the free troposphere, either due to subsiding air masses (such as over northern Africa and the Middle East) or due to active convection (such as over the Caribbean Sea and Gulf Coast of the United States).

Since the O_3 response to CH_4 depends strongly on NO_x, we underscore the need for a better understanding of the global NO_x distribution. A key policy implication from our study is that the efficacy of CH_4 emission reductions for addressing global air quality and climate goals is nearly independent of the location of the emissions. This result is

particularly important given the rising cost of implementing additional controls on the traditional O_3 precursors in many nations where these emissions have already been regulated for decades. Accurate determination of CH_4 emissions by region and sector will nevertheless be critical for estimating the costs and technical feasibility of various options for CH_4 control, as well as for understanding the relative contributions from anthropogenic and natural CH_4 sources.

Acknowledgments

We are grateful to F.J. Dentener for providing the baseline CLE and MFR emissions and J.S. Wang for providing the biogenic emissions, and to E. Baum, J. Chaisson, R.G. Derwent, H. Levy II, R.A. Harley, D.D. Parrish, D. Shindell, S. Sillman, and A. Zuber for insightful discussions. We acknowledge funding from Luce Foundation via Clean Air Task Force.

References

Brasseur, G.P., X.X. Tie, P.J. Rasch, and F. Lefèvre (1997), A three-dimensional simulation of the Antarctic ozone hole: Impact of anthropogenic chlorine on the lower stratosphere and upper troposphere, *J. Geophys. Res., 102*, 8909-8930.

Chameides, W.L., R.W. Lindsay, J. Richardson, C.S. Kiang (1988), The role of biogenic hydrocarbons in urban photochemical smog: Atlanta as a case study, *Science, 241*, 1473-1475.

Carter, W. P. L., and R. Atkinson (1996), Development and evaluation of a detailed mechanism for the atmospheric reactions of isoprene and NO_x, *Int. J. Chem. Kinet., 28*, 497– 530.

Chen, X., D. Hulbert, and P. B. Shepson (1998), Measurement of the organic nitrate yield from OH reaction with isoprene, *J. Geophys. Res., 103*, 25,563– 25,568.

Chen, G., et al. (2005), An investigation of the chemistry of ship emission plumes during ITCT 2002, *J. Geophys. Res., 110*, D10S90, doi:10.1029/2004JD005236.

Cofala, J., M. Amann, Z. Klimont, and W. Sch¨opp (2005) Scenarios of World Anthropogenic Emissions of SO2, NOx, and CO up to 2030, in Internal report of the Transboundary Air Pollution Programme, pp. 17, http://www.iiasa.ac.at/rains/global_emiss/global_emiss.html, International Institute for Applied Systems Analysis, Laxenburg, Austria.

Crutzen, P. (1973), A discussion of the chemistry of some minor constituents in the stratosphere and troposphere, *Pure Appl. Geophys., 106-108*, 1385-1399.

Denman, K.L., et al. (2007), Couplings Between Changes in the Climate System and Biogeochemistry. In: *Climate Change 2007: The Physical Science Basis, Contribution of Working Group I to the Fourth Assessment Report of the Intergovernmental Panel on Climate Change* [Solomon, S. and 7 others (eds.)]. Cambridge University Press, Cambridge, United Kingdom and new York, NY, USA.

Dentener, F., D. Stevenson, J. Cofala, R. Mechler, M. Amann, P. Bergamaschi, F. Raes, and R. Derwent (2005), The impact of air pollutant and methane emission controls on tropospheric ozone and radiative forcing: CTM calculations for the period 1990-2030, *Atmos. Chem. Phys.* **5,** 1731-1755.

Dentener, F., et al. (2006a), Nitrogen and sulfur deposition on regional and global scales: a multi-model evaluation, *Global Biogeochem. Cycles, 20*, GB4003, doi:10.1029/2005GB002672.

Dentener, F., et al. (2006b), The global atmospheric environment for the next generation, *Environ. Sci. Technol., 40*, 3586-3594.

Derwent, R.G., G. Grennfelt, and Ö. Hov (1991), Photochemical oxidants in the atmosphere Nord 1991:7, Nordic Council of Ministers, Copenhagen.

Dlugokencky, E.J., R.C. Myers, P.M. Lang, K.A. Masarie, A.M. Crotwell, K.W. Thoning, B.D. Hall, J.W. Elkens, and L.P. Steele (2005), Conversion of NOAA atmospheric dry air CH4 mole fractions to a gravimetrically prepared standard scale, *J. geophys. Res., 110*, D18306, doi: 10.1029/2005JD006035.

Eder, B.K., J.M. Davis, and P. Bloomfield (1993), A characterization of the spatiotemporal variability of non-urban ozone concentrations over the eastern United States, *Atmos. Environ., 27A*(16), 2645-2668.

EMEP (2005), *EMEP/CCC-Report 1/2005*, Norwegian Institute for Air Research, Norway.

Eyring, V., et al. (2007), Multi-model simulations of the impact of international shipping on Atmospheric Chemistry and Climate in 2000 and 2030, *Atmos. Chem. Phys., 7*, 757-780.

Fiore, A. M., D.J. Jacob, B.D. Field, D.G. Streets, S.D. Fernandes, and C. Jang (2002a), Linking Air Pollution and Climate Change: The Case for Controlling Methane, *Geophys. Res. Lett.* **29,** 1919.

Fiore, A.M., D.J. Jacob, I. Bey, R.M. Yantosca, B.D. Field, A.C. Fusco, and J.G. Wilkinson (2002b), Background ozone over the United States in Summer: Origin, trend, and contribution to pollution episodes, *J. Geophys. Res., 107* (D15), doi:10.1029/2001JD000982.

Fiore, A.M., D.J. Jacob, H. Liu, R.M. Yantosca, T.D. Fairlie, Q. Li (2003), Variability in surface ozone background over the United States: Implications for air quality policy, *J. Geophys. Res. 108,* 4787, doi:10.1029/2003JD003855.

Fiore, A.M., L.W. Horowitz, D.W. Purves, H. Levy II, M.J. Evans, Y. Wang, Q. Li, and R.M. Yantosca (2005), Evaluating the contribution of changes in isoprene emissions to surface ozone trends over the eastern United States, *J. Geophys. Res., 110*, D12303, doi:10.1029/2004JD005485.

Fiore A.M., L.W. Horowitz, E.J. Dlugokencky, and J.J. West (2006), Impact of meteorology and emissions on methane trends, 1990-2004, *Geophys. Res. Lett. 33*, L12809, doi:10.1029/2006GL026199.

Freidenreich, S. M., and V. Ramaswamy (1999), A new multiple-band solar radiative parameterization for general circulation models, *J. Geophys. Res., 104*, 31389-31409.

Geophysical Fluid Dynamics Laboratory (GFDL) Global Atmospheric Model Development Team (GAMDT) (2004), The new GFDL global atmosphere and land model AM2-LM2: Evaluation with prescribed SST simulations, *J. Climate, 17*, 4641-4673.

Hansen, J., M. Sato, R. Ruedy, A. Lacis, V. Oinas (2000), Global warming in the twenty-first century: An alternative scenario, *PNAS 97*, 9875-9880, doi:10.1073/pnas.170278997.

Henderson, S. C., et al. (1999), Aircraft emissions: Current inventories and future scenarios, in IPCC Special Report: Aviation and the Global Atmosphere, edited by J. E. Penner et al., pp. 290 – 331, Cambridge Univ.Press, New York.

Horowitz, L. W., et al. (2003), A global simulation of tropospheric ozone and related tracers: Description and evaluation of MOZART, version 2, *J. Geophys. Res.*, *108*(D24), 4784, doi:10.1029/2002JD002853.

Hough, A.M., and R.G. Derwent (1987), Computer Modelling Studies of the Distribution of Photochemical Ozone Production Between Different Hydrocarbons, *Atmos. Environ. 21(9)*, 2015-2033.

Jacob, D. J., et al. (1993), Simulation of summertime ozone over North America, *J. Geophys. Res., 98(D8)*, 14,797–14,816.

Kalnay, E. et al. (1996), The NCEP/NCAR 40-year reanalysis project, *Bull. Amer. Meteor. Soc.*, *77*, 437-470.

Kasibhatla, P., et al. (2000), Do emissions from ships have a significant impact on concentrations of nitrogen oxides in the marine boundary layer? *Geophys. Res. Lett. 27(15),* 2229-2232, doi:10.1029/2000GL011387.

Lawrence, M.G., P. Jöckel, R. von Kuhlmann (2001), What does the global mean OH concentration tell us? *Atmos. Chem. Phys., 1*, 37-49, www.atmos-chem-phys.org/acp/1/37/.

Levy, H. II, M.D. Schwarzkopf, L.W. Horowitz, V. Ramaswamy, and K. Findell (2007), Strong Sensitivity of Late 21st Century Climate to Projected Changes in Short-lived Air Pollutants, submitted to *J. Geophys. Res*.

Li, Q., et al. (2002), Transatlantic transport of pollution and its effects on surface ozone in Europe and North America, *J. Geophys. Res.*, *107*, 4166, 10.1029/2001JD001422.

Liang, J., and M.Z. Jacobson (2000), Effects of subgrid segregation on ozone production efficiency in a chemical model, *Atmos. Environ., 34*, 2975-2982.

Logan, J.A. (1989), Ozone in rural areas of the United States, *J. Geophys. Res., 94*, 8511-8532.

Marenco, A., H. Gouget, P. Nedelec, J.P. Pages and F. Karcher (1994), Evidence of a long-term increase in tropospheric ozone from Pic du Midi data series: Consequences: Positive radiative forcing, *J. Geophys. Res.* **99,** 16617-16632.

Martien, P.T., and R.A. Harley (2006), Adjoint Sensitivity Analysis for a Three-Dimensional Photochemical Model: Application to Southern California, *Env. Sci. Technol., 40*, 4200-4210.

Murazaki, K. and P. Hess (2006), How does climate change contribute to surface ozone change over the United States?, *J. Geophys. Res., 111*, D05301, doi:10.1029/2005JD005873.

Nakicenovic, N., et al. (2000), Special Report on Emissions Scenarios, Intergovernmental Panel on Climate Change, pp. 599, Cambridge University press, Cambridge, United Kingdom and New York, USA.

Naik, V., D. Mauzerall, L. Horowitz, M. D. Schwarzkopf, V. Ramaswamy, and M. Oppenheimer (2005), Net radiative forcing due to changes in regional emissions of tropospheric ozone precursors, *J. Geophys. Res., 110*, D24306, doi:10.1029/2005JD005908.

Naik, V., D. Mauzerall, L. Horowitz, M. D. Schwarzkopf, V. Ramaswamy, and M. Oppenheimer (2007), On the sensitivity of radiative forcing from biomass burning aerosols and ozone to emission location, *Geophys. Res. Lett., 34* , L03818, doi:10.1029/2006GL028149.

Olivier, J.G.J., A.F. Bouwman, C.W.M. Van der Maas, J.J.M. Berdowski, C. Veldt, J.P.J. Bloos, A.J.H. Visschedijk, P.Y.J. Zandveld and J.L. Haverlag (1996), Description of EDGAR Version 2.0: A set of global emission inventories of greenhouse gases and ozone-depleting substances for all anthropogenic and most natural sources on a per country basis and on 1ox1o grid. National Institute of Public Health and the Environment (RIVM) report no. 771060 002 / TNO-MEP report no. R96/119.

Olivier, J.G.J, A.F. Bouwman, J.J.M. Berdowski, C. Veldt, J.P.J. Bloos, A.J.H. Visschedijk, C.W.M. van der Maas and P.Y.J. Zandveld (1999), Sectoral emission inventories of greenhouse gases for 1990 on a per country basis as well as on 1x1 degree. *Environmental Science & Policy, 2,* 241-264.

Prather, M. J. (1996), Time scales in atmospheric chemistry: Theory, GWPs for CH_4 and CO, and runaway growth, *Geophys. Res. Lett., 23*, 2597-2600.

Prather, M., et al. (2001), in *Climate Change 2001: The Scientific Basis*, eds. Houghton, J. T., Ding, Y., Griggs, D. J., Noguer, M., van der Linden, P. J., Dai, X., Maskell, K. & Johnson, C. A. (Cambridge University Press, Cambridge), pp. 239-287.

Ramaswamy, V., Boucher, O., Haigh, J., Hauglustaine, D., Haywood, J., Myhre, G., Nakajima, T., Shi, G. Y. & Solomon, S. (2001), in *Climate Change 2001: The Scientific Basis*, eds. Houghton, J. T., Ding, Y., Griggs, D. J., Noguer, M., van der Linden, P. J., Dai, X., Maskell, K. & Johnson, C. A. (Cambridge University Press, Cambridge), pp. 349-416.

Ravishankara A.R., Dunlea E.J., Blitz M.A., T. J. Dillon, D. E. Heard, M. J. Pilling, R. S. Strekowski, J. M. Nicovich, and P. H. Wine (2002), Redetermination of the rate coefficient for the reaction of $O(^1D)$ with N_2, *Geophys. Res. Lett.*, *29* (15), 1745.

Roehl C.M., et al. (2002), Photodissociation of peroxynitric acid in the near-IR, *J. Phys. Chem. A 106* (15), 3766-3772.

Schwarzkopf, M. D., and V. Ramaswamy (1999), Radiative effects of CH_4, N_2O, halocarbons and the foreign-broadened H_2O continuum: A GCM experiment, *J. Geophys. Res.*, *104*, 9467-9488.

Shindell, D. T., G. Faluvegi, N. Bell, and G. A. Schmidt (2005), An emissions-based view of climate forcing by methane and tropospheric ozone, *Geophys. Res. Lett.*, *32*, L040803.

Shindell, D.T., et al. (2006), Multi-model simulations of carbon monoxide: Comparison with observations and projected near-future changes, *J. Geophys. Res.*, *111*, D19306, doi:10.1029/2006JD007100.

Spivakovsky, C.M., et al. (2000), Three-dimensional climatological distribution of tropopsheric OH: Update and evaluation, *J. Geophys. Res.*, *105 (D7)*, 8931-8980.

Sprengnether, M., K. L. Demerjian, N. M. Donahue, and J. G. Anderson (2002), Product analysis of the OH oxidation of isoprene and 1,3-butadiene in the presence of NO, *J. Geophys. Res.*, *107(D15)*, 4268, doi:10.1029/2001JD000716.

Stevenson, D.S., et al. (2006), Multi-model ensemble simulations of present-day and near-future tropospheric ozone, *J. Geophys. Res.*, *111*, D08301, doi:10.1029/2005JD006338.

Task Force on Hemispheric Transport of Air Pollution (TF HTAP) (2007), Interim report, available at www.htap.org.

Van der Werf, G.R., J.T. Randerson, G.J. Collatz, and L. Giglio (2003), Carbon emissions from fires in tropical and subtropical ecosystems, *Global Change Biology, 9*, 547-562.

van Noije, T.P.C., et al. (2006) Multi-model ensemble simulations of tropospheric NO2 compared with GOME retrievals for the year 2000, *Atmos. Chem. Phys., 6(10)*, 2943-2979.

Wang, J.S., J. A. Logan, M. B. McElroy, B. N. Duncan, I. A. Megretskaia, R. M. Yantosca (2004), A 3-D model analysis of the slowdown and interannual variability in the methane growth rate from 1988 to 1997, *Global Biogeochem. Cycles, 18*, GB3011, doi:10.1029/2003GB002180.

Wang, Y. H. and Jacob, D. J. (1998) Anthropogenic forcing on tropospheric ozone and OH since preindustrial times, *J. Geophys. Res.* **103,** 31123-31135.

West, J.J. and A.M. Fiore (2005), Management of Tropospheric Ozone by Reducing Methane Emissions, *Environ. Sci. & Technol., 39,* 4685-4691.

West, J. J., A. M. Fiore, L. W. Horowitz, and D. L. Mauzerall (2006), Global health benefits of mitigating ozone pollution with methane emission controls, *Proc. Natl. Acad. Sci. U. S. A., 103,* 3988-3993.

West, J. J., A. M. Fiore, V. Naik, L.W. Horowitz, M.D. Schwarzkopf, D.L. Mauzerall (2007a), Ozone air quality and radiative forcing consequences of changes in ozone precursor emissions, *Geophys. Res. Lett., 34* , L06806, 10.1029/2006GL029173.

West, J.J. et al. (2007b), Management of tropospheric ozone by reducing methane emissions: comparison of abatement costs and global mortality benefits under future methane abatement scenarios, manuscript in prep.

Table 1: Description of MOZART-2 Simulations

Simulation name	CH_4 Emissions or Mixing Ratio	Non-CH_4 O_3 Precursor Emissions	NCEP years
Transient Simulations			
BASE	BASE (see Table 2)	BASE	1990-2004, recycled once
RGLOB	BASE with anthropogenic emissions[a] reduced by 97 Tg yr^{-1}		1990-2004, recycled once
RASIA	BASE with anthropogenic emissions[a] in Asia set to zero (-97 Tg yr^{-1})		1990-2000[d]
CLE[b]	CLE 2005-2030 (Table 2; Figure 2a)	CLE	2000-2004, recycled five times for the 2005-2030 period
A	CLE 2005-2030 with 75 Tg yr^{-1} decrease[c] by 2030 (Figure 2a)		
B	CLE 2005-2030 with 125 Tg yr^{-1} decrease[c] by 2030 (Figure 2a)		
C	CLE 2005-2030 with 180 Tg yr^{-1} decrease[c] by 2030 (Figure 2a)		
Steady-state Simulations			
GLOB1760	$[CH_4]$=1760 ppb	BASE	2000
GLOB1460	$[CH_4]$=1460 ppb		
FT1460	$[CH_4]$=1460 ppb above 724 hPa; $[CH_4]$=1760 ppb elsewhere		
PBL1460	$[CH_4]$=1760 ppb above 724 hPa; $[CH_4]$=1460 ppb elsewhere		
CH_4-700	$[CH_4]$=700 ppb	CLE year 2030	

[a]Anthropogenic emissions are as defined in Table 2 but exclude agricultural waste burning. The 97 Tg yr^{-1} reduction in BASE is applied to the anthropogenic emissions as a globally uniform decrease of 39%.
[b]Current Legislation Scenario [*Dentener et al*., 2005].
[c]The anthropogenic (industrial plus agricultural) CLE CH_4 emissions were scaled to the desired emission reduction according to the spatial pattern of the difference between CH_4 emissions in the CLE and "Maximum technologically Feasible Reduction" (MFR) scenarios in 2030 from *Dentener et al*. [2005].
[d]The RASIA simulation was stopped after 11 years since there was little difference in the O_3 response from that in RGLOB.

Table 2: Methane emissions (Tg CH_4 yr^{-1}) used in this study

	BASE	Current Legislation (CLE)			
Year	1990s	2005	2010	2020	2030
Anthropogenic	308[a]	332[d]	364 [d]	397 [d]	428 [d]
Natural[b]	214	222	222	222	222
Biomass Burning[c]	25	23	23	23	23
Total	547	577	609	642	673

[a]Emissions in the BASE simulation include energy use, landfills, wastewater, rice, ruminants, and agricultural waste burning from the EDGAR v2.0 inventory [*Olivier et al*., 1996; 1999] as described in *Horowitz et al*. [2003].
[b]Includes 10 Tg yr^{-1} from oceans. The distribution and seasonality of the wetland emissions are from *Horowitz et al*. [2003] in BASE, and from *Wang et al*. [2004] in CLE.
[c]For BASE, biomass burning of savannas and forests is from *Horowitz et al*. [2003]. The CLE simulations use biomass burning from the Global Fire Emissions Database (GFEDv1) climatology for 1997-2002 [*van der Werf et al*., 2003].
[d]Includes anthropogenic CH_4 emissions separated into agricultural and industrial sectors as specified in the CLE inventory [*Dentener et al*., 2005].

Table 3. Spatial distribution of CH_4 loss by reaction with OH (BASE simulation) and change in gross tropospheric O_3 production (RGLOB-BASE simulations).

	90-30S	30-0S	0-30N	30-90N	*Total*
Methane loss by reaction with OH (%)					
500-250 hPa	1.2	3.4	4.0	1.8	*10.4*
750-500 hPa	3.2	11.3	13.1	5.3	*32.9*
Surface-750 hPa	4.4	18.9	23.6	9.8	*56.7*
Total	*8.8*	*33.6*	*40.7*	*16.9*	*100*
Change in gross ozone production (Tg yr^{-1})					
500-250 hPa	-5.5	-11.5	-14.3	-8.4	*-39.7*
750-500 hPa	-5.8	-23.1	-26.3	-11.3	*-66.5*
Surface-750 hPa	-7	-23.5	-30.5	-23	*-84*
Total	*-18.3*	*-58.1*	*-71.1*	*-42.7*	*-190.2*

Table 4. Adjusted radiative forcing (W m^{-2}) in 2030 versus 2005 due to changes in tropospheric CH_4 and O_3.

Simulation	CH_4[1]	O_3[2]
CLE	0.099	0.065
A	0.033	0.048
B	-0.029	0.032
C	-0.097	0.014
CH_4-700	-0.501	-0.080

[1]Calculated with the analytic expression from *Ramaswamy et al*. [2001].
[2]Calculated in the GFDL AM2 radiative transfer model, including stratospheric adjustment following the approach of *Naik et al*. [2007]. The tropospheric O_3 forcing is dominated by longwave radiation, with a 21-25% contribution from shortwave.

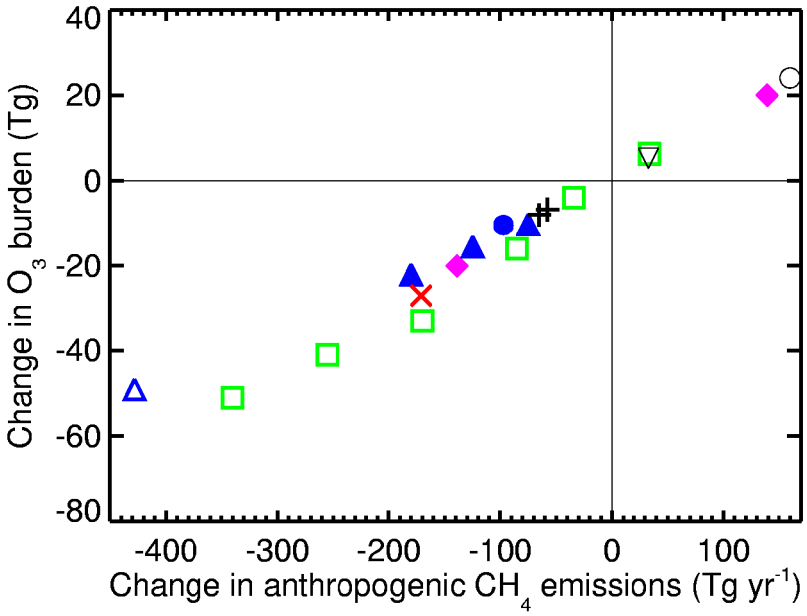

Figure 1. The change in tropospheric O_3 burden (Tg) as a function of the change in anthropogenic CH_4 emissions (Tg yr^{-1}), compiled from modeling studies in the literature encompassing a range of modeling approaches: (1) full-chemistry, transient simulations (pink filled diamonds: TM3 [*Dentener et al.*, 2005]; blue filled circle: RGLOB-BASE in this work; blue filled triangles: 2030 results from future scenarios A, B, and C in this work), (2) steady-state simulations in which a uniform, fixed CH_4 concentration is adjusted to reflect a change in CH_4 emissions (red x: GEOS-Chem [*Fiore et al.*, 2002a]; black upside down triangle: recommended based on IPCC TAR models, with the O_3 burden change reduced by 25% to correct for the inclusion of stratospheric O_3 in the reported results [*Prather et al.*, 2001]; black +: MOZART-2 [*West et al.*, 2006, 2007a]; open black circle: addition of CH_4 to the pre-industrial atmosphere in a global CTM [*Wang and Jacob*, 1998]; open blue triangle: CH_4-700 simulation in this work), and (3) a hybrid approach where the initial CH_4 trends from a transient simulation were extrapolated exponentially using the model's CH_4 perturbation time of 12.6 years, followed by 5 additional years of simulation (green squares: GISS [*Shindell et al.*, 2005 and personal communication, 2006]). All blue symbols (from RGLOB-BASE and the differences of the 2030 A, B, C, CH_4-700 and 2030 CLE simulations) denote the O_3 burden change adjusted to steady state as described in Section 3. The two left-most points depict simulations in which anthropogenic CH_4 emissions are eliminated.

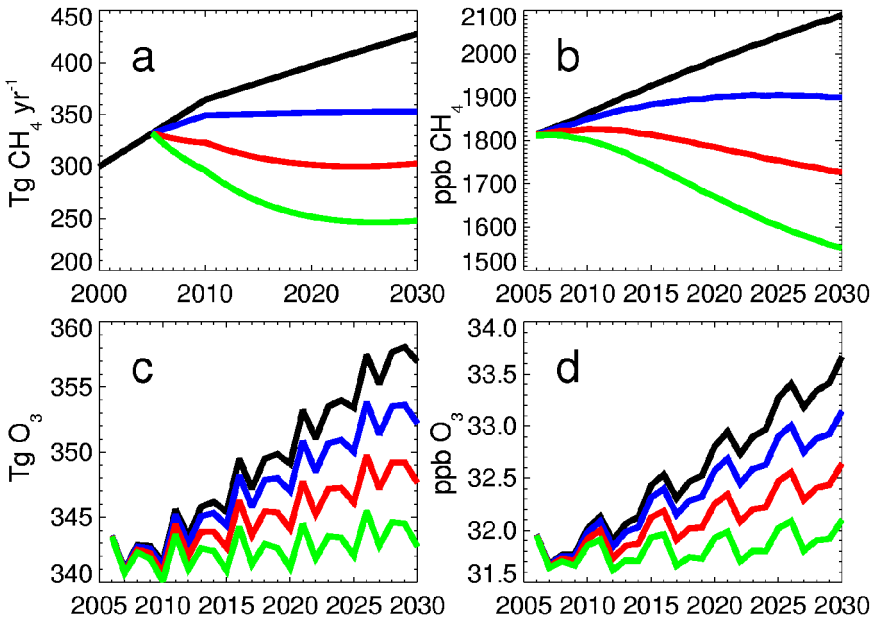

Figure 2. (a) Anthropogenic CH_4 emissions (Tg yr^{-1}), (b) annual mean surface CH_4 mixing ratios in dry air (nmol mol^{-1}, abbreviated ppb) (c) annual mean tropospheric O_3 burden (Tg), and (d) 8-hour daily maximum (MDA8) O_3 concentrations (ppb) under the CLE scenario (black), and following CH_4 control scenarios A (blue), B (red), and C (green), described in Section 2.2. The 150 ppb O_3 chemical tropopause in 2005 is used to calculate the tropospheric O_3 burden.

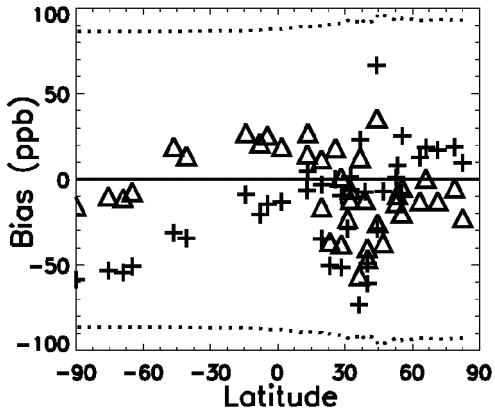

Figure 3. Annual mean bias (MOZART-2 model – NOAA observations) for CH_4 abundance in dry surface air (ppb) in 2004, for year 15 of the BASE simulation (crosses) and the final year of a 5-year spin-up for the CLE simulations (triangles). The selected model years for both simulations use the 2004 NCEP meteorology. The model always falls within ±5% of the observed values (dotted lines).

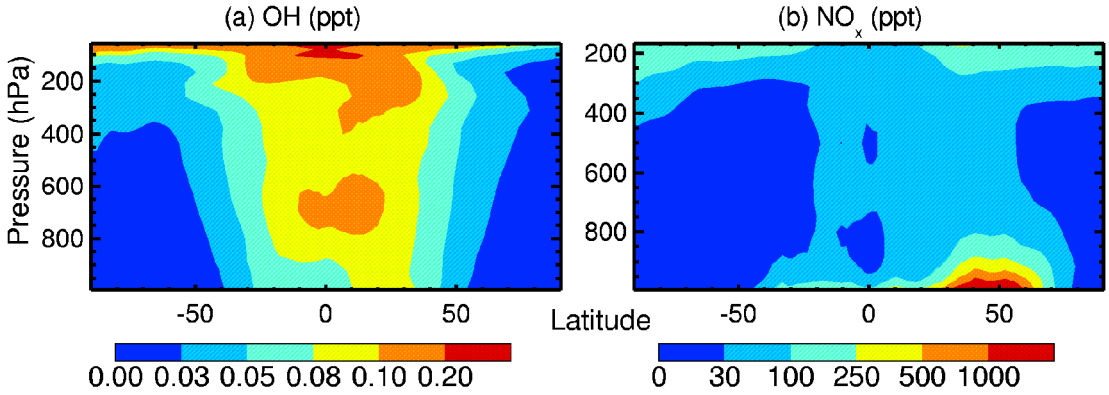

Figure 4. Zonal annual mean distributions of (a) OH and (b) NO_x (ppt) in the BASE simulation in year 30.

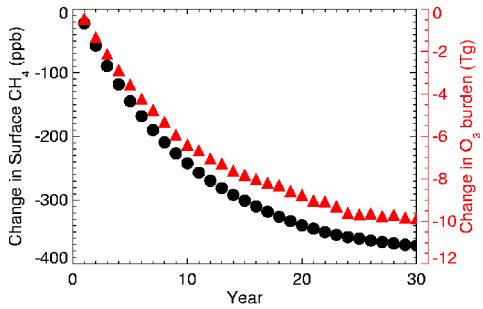

Figure 5. Annual mean change in surface CH_4 abundances (black circles; left axis) and in the tropospheric O_3 burden (red triangles; right axis), resulting from a 97 Tg yr^{-1} decrease in global anthropogenic CH_4 emissions relative to values in the same year of the BASE simulation (RGLOB-BASE) to remove the interannual variability due to meteorology. The 150 ppb O_3 chemical tropopause in the first year of the BASE simulation is used to calculate the tropospheric O_3 burden. In the first year of the BASE simulation, the total tropospheric O_3 burden is 300 Tg and the surface CH_4 abundance is 1720 ppb.

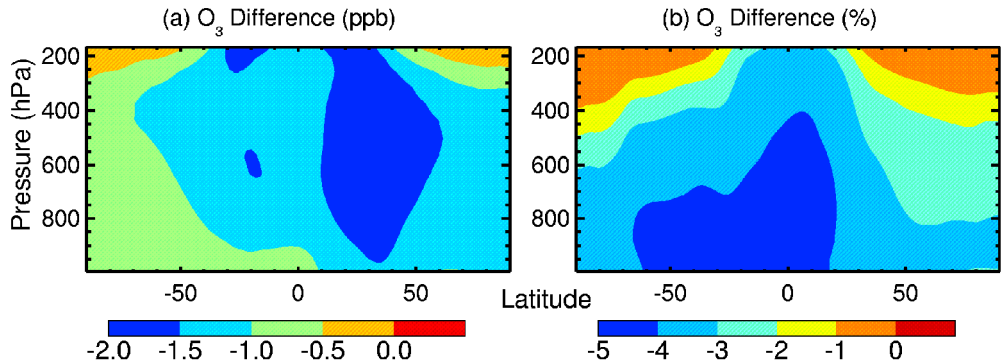

Figure 6. (a) Absolute and (b) percentage change in zonal annual mean O_3 in year 30 due to a sustained 97 Tg yr^{-1} reduction in global anthropogenic CH_4 emissions (RGLOB-BASE).

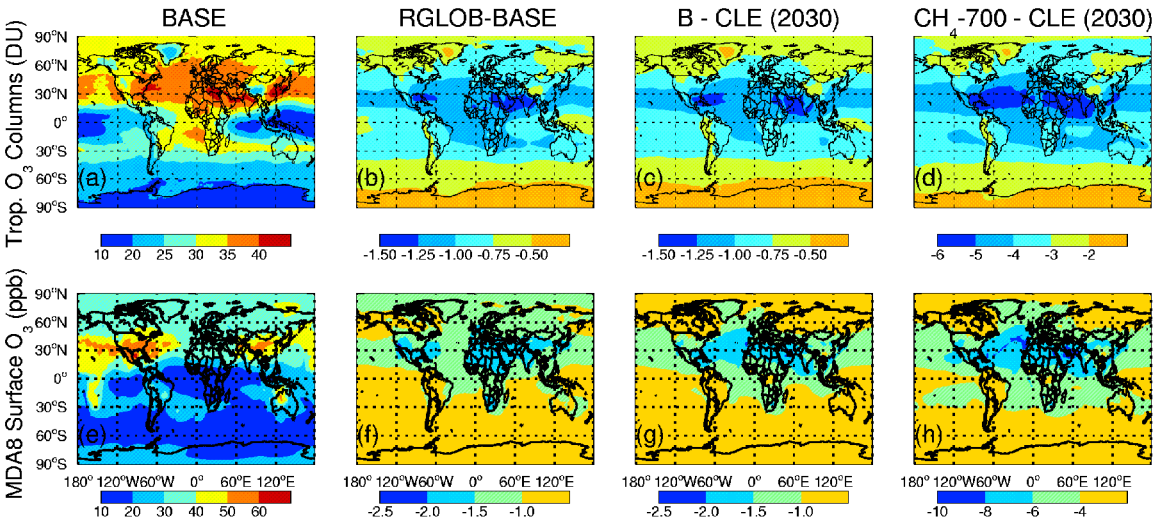

Figure 7. Annual mean tropospheric O_3 columns (top row) and 8-hour daily maximum (MDA8) O_3 concentrations in surface air (bottom row) in the BASE simulation (a,e) and the change resulting from decreases in global anthropogenic CH_4 emissions: RGLOB-BASE in year 30 (b,f), Scenario B – CLE in 2030 (c,g), and CH_4-700 – CLE in 2030 (d,h). Note the different color scales for the CH_4-700 results. Tropospheric O_3 columns are calculated using the 150 ppb O_3 chemical tropopause in BASE year 30 for the BASE and RGLOB simulations, and the CLE 2030 chemical tropopause for the CLE, B, and CH_4-700 simulations.

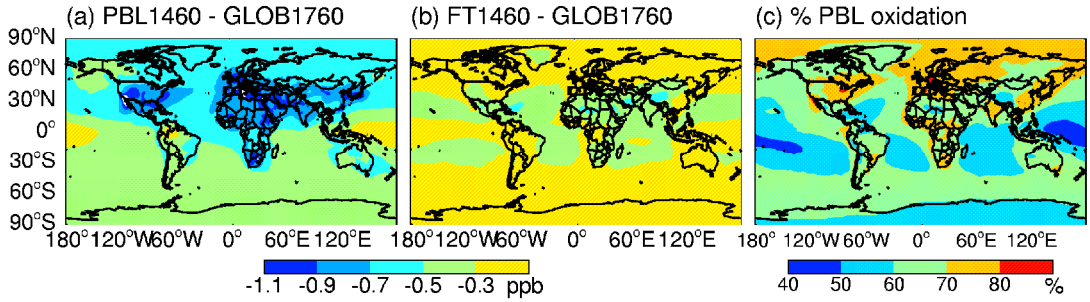

Figure 8. Change in annual mean MDA8 surface O_3 (ppb) from reducing CH_4 concentrations by 300 ppb (a) within the boundary layer (below 724 hPa) and (b) within the free troposphere, as diagnosed from steady-state simulations (PBL1460-GLOB1760) and (FT1460-GLOB1760), respectively (Table 1). (c) Percentage contribution from CH_4 oxidation within the planetary boundary layer to the total surface O_3 change from CH_4 reductions. White space in (a) indicates changes < -1.1 ppb (max change of -1.7); the full range in (c) is 45-87%.

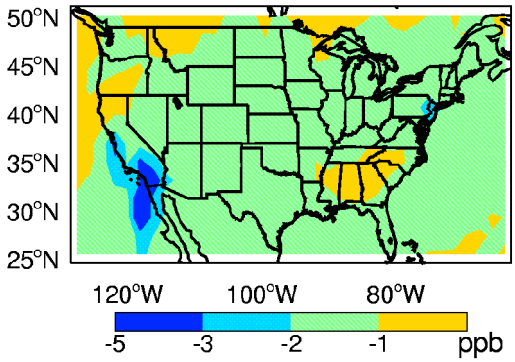

Figure 9. Composite maximum change in U.S. MDA8 surface O_3 occurring in each model grid cell on any day between June 1 to August 31 from reducing CH_4 concentrations by 300 ppb within the boundary layer (below 724 hPa; PBL1460-GLOB1760).

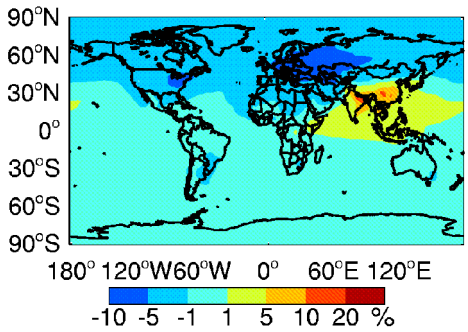

Figure 10. The percentage difference of the change in annual mean MDA8 surface O_3 in simulation year 11 in the RASIA and RGLOB simulations, calculated as 100*(RASIA-RGLOB)/(RGLOB-BASE). Values range from -9 to +20.

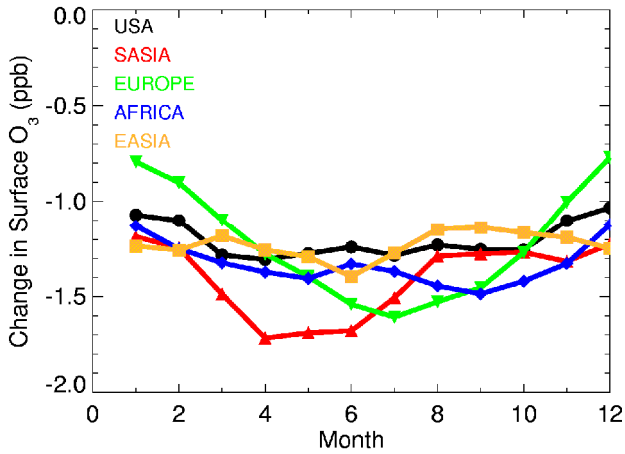

Figure 11. Monthly mean change in surface O_3 over land boxes (≥50% land) in selected regions, resulting from a sustained 97 Tg yr^{-1} reduction in global anthropogenic CH_4

emissions after 30 years of simulation (RGLOB-BASE). The regions are defined as: USA (62.5-127.5°W; 24-52°N), EUROPE (10°W-50°E; 35-70°N); SOUTH ASIA (50-100°E; 5-35°N), EAST ASIA (100-150°E; 25-50°N); AFRICA (20°W-50°E; 35°S-35°N).

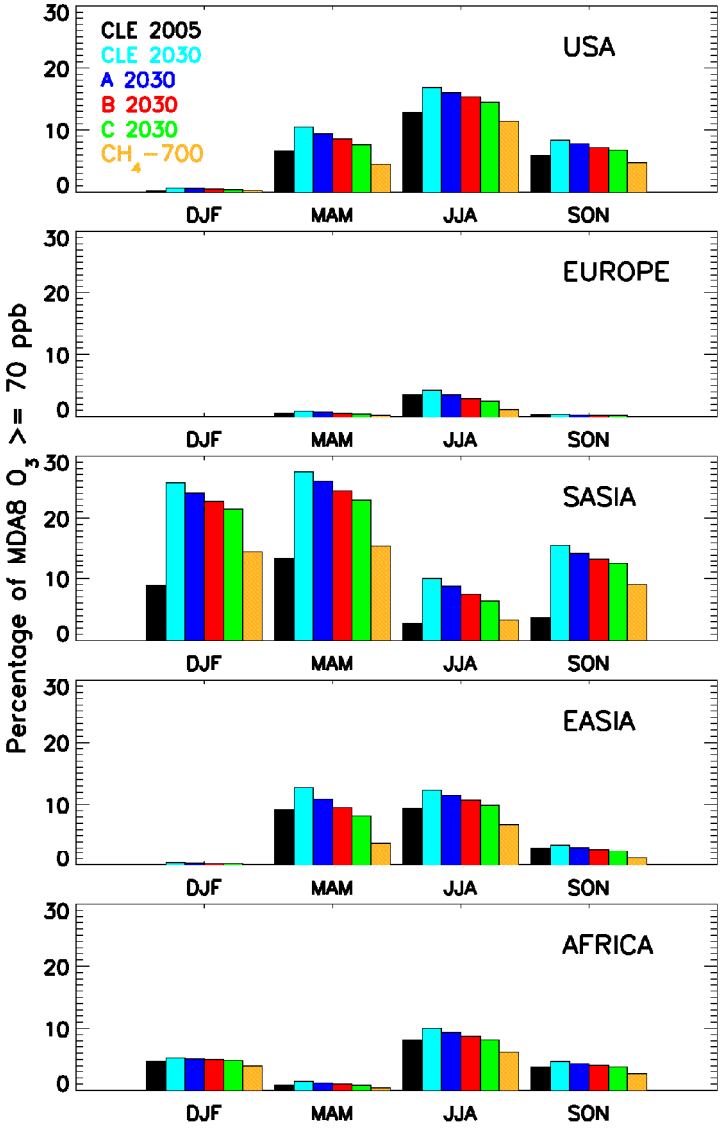

Figure 12. Percentage of model grid-cell days with MDA8 surface O_3 concentrations ≥ 70 ppb by season and region for the future scenarios described in section 2.2: CLE 2005 (black); CLE 2030 (cyan); A (blue), B (red), and C (green) in 2030; and CH_4-700 (orange). The regions are defined in the caption to Figure 11.

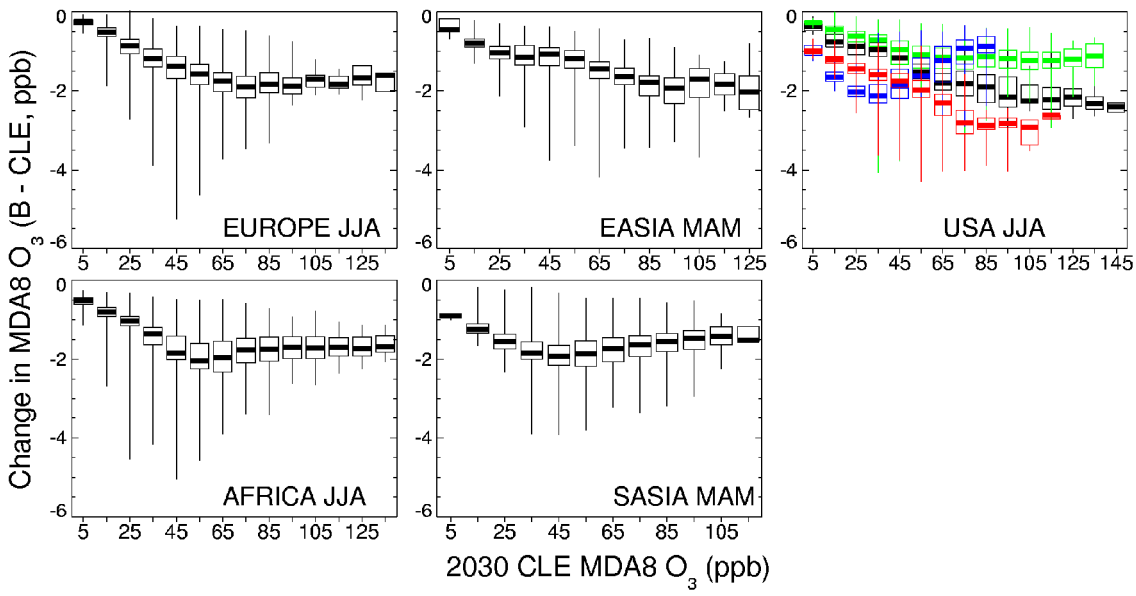

Figure 13. Change in MDA8 surface O_3 concentrations in 2030 resulting from the CH_4 controls in Scenario B (B – CLE), plotted against the MDA8 O_3 values in 2030 in the baseline CLE scenario, for each 10 ppb bin. The boxes enclose the 25th-75th percentiles, with the median denoted by the thick horizontal line. Vertical lines represent the full range of values for each bin. The distribution is constructed from the 92 daily values from each grid cell in the region for summer (Europe, Africa, USA) or spring (East Asia and South Asia). Region boundaries are given in the caption to Figure 11. The USA is subdivided into quadrants at 100°W and 35°N: northeast (green), southeast (blue), southwest (red), and northwest (black).

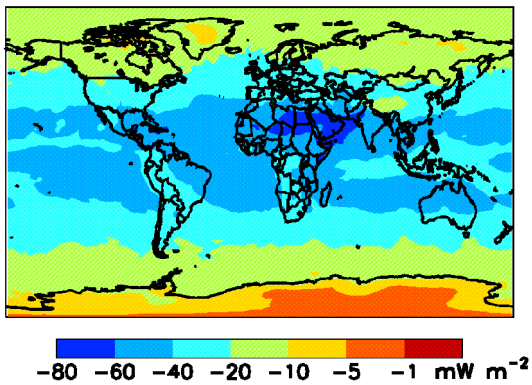

Figure 14. Adjusted radiative forcing from tropospheric O_3 in scenario B relative to the CLE baseline, for the year 2030 (mW m^{-2}).